MOLECULAR IMAGING AND BIOLOGY

Mol Imaging Biol (2020) 22:367–376
DOI: 10.1007/s11307-019-01386-7

Published Online: 17 June 2019

WMIS World Molecular Imaging Society
esmi European Society for Molecular Imaging

Check for updates

RESEARCH ARTICLE

[^{89}Zr]A2cDb Immuno-PET of Prostate Cancer in a Human Prostate Stem Cell Antigen Knock-in (hPSCA KI) Syngeneic Model

Kirstin A. Zettlitz,[1,2,3] Wen-Ting K. Tsai,[1,2] Scott M. Knowles,[1,2,4] Felix B. Salazar,[1,2] Naoko Kobayashi,[2,5] Robert E. Reiter,[2,5] Anna M. Wu[1,2,3]

[1]*Crump Institute for Molecular Imaging, Department of Molecular and Medical Pharmacology, University of California Los Angeles, Los Angeles, CA, USA*
[2]*David Geffen School of Medicine, University of California Los Angeles, Los Angeles, CA, USA*
[3]*Molecular Imaging and Therapy, Beckman Research Institute, City of Hope, 1500 E. Duarte Rd, Duarte, CA, 91010, USA*
[4]*University of Washington/Fred Hutchinson Cancer Research Center, 1100 Fairview Ave N-D5-100, Seattle, WA, 98109, USA*
[5]*Department of Urology, University of California Los Angeles, Los Angeles, CA, USA*

Abstract

Purpose: A great challenge in the diagnosis and treatment of prostate cancer is distinguishing between indolent or local disease and aggressive or metastatic disease. Antibody-based positron emission tomography (immuno-PET) as a cancer-specific imaging modality could improve diagnosis of primary disease, aid the detection of metastases to regional lymph nodes as well as to distant sites (*e.g.*, bone), and monitor response to therapy.

Procedure: In search for a more physiologically relevant disease model, a human prostate stem cell antigen knock-in (hPSCA KI) mouse model was generated. The use of a syngeneic prostate cancer cell line transduced to express human PSCA (RM-9-hPSCA) enabled the evaluation of anti-PSCA immuno-PET in immunocompetent mice and in the context of normal tissue expression of PSCA. Two PSCA-specific humanized antibody fragments, A11 minibody and A2 cys-diabody, were radiolabeled with positron emitters iodine-124 and zirconium-89, respectively ([^{124}I]A11 Mb and [^{89}Zr]A2cDb), and used for immuno-PET in wild-type, hPSCA KI and tumor-bearing mice.

Results: The hPSCA KI mice express PSCA at low levels in the normal prostate, bladder and stomach, reproducing the expression pattern seen in humans. [^{124}I]A11 Mb immuno-PET detected increased levels of PSCA expression in the stomach, and because I-124 is non-residualizing, very little activity was seen in organs of clearance (liver, kidney, spleen). However, due to the longer half-life of the 80 kDa protein, blood activity (and thus urine activity) at 20 h postinjection remains high. The smaller 50 kDa [^{89}Zr]A2cDb cleared faster, resulting in lower blood and background activity, despite the use of a residualizing radiometal. Importantly, [^{89}Zr]A2cDb immuno-PET showed antigen-specific targeting of PSCA-expressing tumors and minimal nonspecific uptake in PSCA-negative controls.

Correspondence to: Kirstin Zettlitz; *e-mail:* kzettlitz@coh.org

Conclusion: Tracer biodistribution was not significantly impacted by normal tissue expression of PSCA. [^{89}Zr]A2cDb immuno-PET yielded high tumor-to-blood ratio at early time points. Rapid renal clearance of the 50 kDa tracer resulted in an unobstructed view of the pelvic region at 20 h postinjection that would allow the detection of cancer in the prostate.

Key Words: Prostate stem cell antigen (PSCA), Immuno-PET, Prostate cancer, Antibody fragment, Minibody, Diabody, Zirconium-89, Iodine-124

Introduction

Currently, prostate biopsies are the only means for definitive diagnosis for prostate cancer (PCa), though imaging is playing an increasing role in the early detection, staging, risk stratification, and disease management of PCa [1, 2]. To improve noninvasive PCa imaging, targets that are cancer specific, accessible, and reliable biomarkers need to be identified. Potential imaging agents require preclinical evaluation in models that enable proof-of-concept testing and generate useful knowledge that can be translated towards better outcomes for patients [3].

Prostate stem cell antigen (PSCA) is a GPI-anchored glycoprotein that is overexpressed on the cell surface of virtually all localized prostate cancers, on prostate cancer bone metastases and on the majority of metastases to other sites [4]. PSCA expression correlates with the Gleason score, metastases, and aggressiveness. Furthermore, PSCA is regulated by androgens and is downregulated as a result of androgen deprivation therapy, while androgen-independent cancers overexpress PSCA [5]. PSCA expression in normal tissues is restricted to the stomach, bladder, and prostate, and no expression is found in bone or lymph nodes where prostate cancer metastasizes to most frequently. These characteristics make PSCA a promising target for both imaging and therapy [6].

Antibody-based positron emission tomography (immuno-PET) offers antigen specific, noninvasive, and quantitative whole-body imaging by combining antibody specificity with the resolution and sensitivity of PET [7–9]. The choice of antibody or antibody fragment and radionuclides enables predetermination of the tracer's metabolism and clearance route. Fc-engineering and molecular weight of the protein impact the half-life and direct clearance to kidneys or liver. Conjugation with non-residualizing (I-124) *vs* residualizing (Zr-89) radionuclides determines the fate of internalized radiometabolites [10].

The anti-human PSCA antibody (1G8) that has been shown to inhibit tumor growth [5, 11] was previously humanized by CDR grafting (2B3) [6, 12] and affinity matured using yeast display [13]. Two antibody fragments were engineered; the A11 minibody (A11 Mb), an 80 kDa scFv-C_H3 dimer, and the A2 cys-diabody (A2cDb), a 50 kDa scFv dimer functionalized with C-terminal cysteine residues. Both antibody fragments have been successfully used for immuno-PET of a variety of prostate cancer cell line xenograft models as well as pancreatic patient–derived xenograft models [10, 13–15].

In search for a more physiologically relevant disease model, a human PSCA knock-in (hPSCA KI) mouse model was used to assess the impact of normal tissue expression of PSCA on the biodistribution of two different-sized PSCA-specific antibody fragments by immuno-PET. [^{124}I]A11 Mb had previously shown superior imaging contrast compared with [^{89}Zr]A11 Mb in xenograft studies and was used in this work to image normal tissue expression of hPSCA in the knock-in mice. We hypothesized that the smaller A2 cys-diabody labeled with a radiometal ([^{89}Zr]A2cDb) would enable imaging at earlier time points due to the combination of its shorter plasma half-life and antigen-specific tissue retention. Furthermore, the syngeneic murine PCa cell line RM-9 transduced to express human PSCA was grown as syngeneic subcutaneous grafts in hPSCA KI mice, and [^{89}Zr]A2cDb was evaluated for PSCA-specific tumor targeting in the context of normal PSCA background.

Materials and Methods

Cell Lines and Mouse Model

The protocols for animal studies were approved by the University of California (UCLA) Chancellor's Animal Research Committee.

The mouse prostate cancer cell line RM-9 and RM-9-hPSCA-Fluc were provided by the University of Texas MD Anderson Cancer Center and Dr. Saul Priceman (City of Hope). Cells were cultured in DMEM, 10 % FBS, and 1 % PSG and maintained in a humidified incubator a 37 °C and 5 % CO_2.

The human PSCA knock-in (hPSCA KI) mouse model was generated by targeted insertion of hPSCA cDNA through homologous recombination in murine embryonic stem cells by standard gene-targeting methods and back-crossing onto C57BL/6J as previously described [16].

Subcutaneous tumors were inoculated by implanting 5×10^4 cells in 100 µl (1:1 PBS:Matrigel) and allowed to grow for 7–10 days.

Anti-PSCA Antibody Fragments

The design, cloning, production, and purification of the humanized, affinity matured human PSCA-specific antibody

fragments A11 Mb and A2cDb has been described previously [13, 17].

Radioiodination of A11 Mb

Iodine-124 labeled A11 minibody ([^{124}I]A11 Mb) was prepared by direct iodination using Pierce® Pre-coated Iodination Tubes (Thermo Scientific) according to the manufacturer's instructions. Approximately 100 μg of protein were incubated with 15 MBq (400 μCi) of Na[^{124}I]I (IBA Molecular) in 0.1 TRIS, pH 8.0 as previously described [10].

Radiolabeling of A2cDb

A2cDb (30 μM in 50 μl PBS) was reduced by incubation with a 10-fold excess of tris(2-carboxyethyl)phosphine (Pierce) for 1 h at room temperature. A 10-fold molar excess of deferoxamine-maleimide (B-772, Macrocyclics) was added and incubated for 2 h at room temperature. Micro Bio-Spin® size exclusion spin columns (Bio-Rad) were used for the removal of excess chelator. Chelation of Zr-89 was achieved by incubating 100 μg of malDFO-labeled protein (A2cDb-malDFO) with 15 MBq (400 μCi) of [^{89}Zr]oxalate (3D imaging) in 1 M HEPES for 1 h at room temperature.

Purification and Characterization of Radiolabeled Antibody Fragments

Removal of free radiolabel (I-124 or Zr-89) and buffer exchange was performed using Micro Bio-Spin® size exclusion spin columns (Bio-Rad). Labeling efficiency and radiochemical purity were assessed by instant thin-layer chromatography (ITLC strips for antibody preparation, Biodex Medical Systems) and saline (I-124) or citric acid (Zr-89) as solvent. Immunoreactivity was measured by incubating radiolabeled antibody fragments with excess antigen-expressing cells (RM-9-PSCA) or control cells (RM-9). Cells and supernatant were separated and measured by gamma counting (Wizard 3″ automated gamma counter; PerkinElmer).

Immuno-PET/CT Imaging

Prior to I-124 immuno-PET of hPSCA KI mice, uptake of radioiodine in thyroid and stomach were blocked by adding Lugol's iodine to the drinking water and by gavage with potassium perchlorate, respectively, as previously described [13]. Thirty micrograms (4.44 MBq/120 μCi) of [^{124}I]A11 Mb or 15 μg (2.8 MBq/75 μCi) of [^{89}Zr]malDFO-A2cDb were injected into the tail vein. Mice were anesthetized with 1.5–2 % isoflurane, bladders were manually expressed, and 10-min static PET scans were acquired (Inveon PET; Siemens and Focus 220 PET; Concorde Microsystems) followed by CT scans (microCAT II; ImTek and CrumpCAT; UCLA in-house small-animal CT scanner). The PET images were reconstructed using non-attenuation corrected filtered-back-projection (FBP) or maximum *a posteriori* (MAP) and presented as whole-body maximum intensity projection (MIP) PET/CT overlays. AMIDE was used for image analysis [18].

Ex Vivo Biodistribution

Dissected tissues were gamma counted, radioactivity was divided by tissue weight, and using the decay-corrected injected dose, percent injected dose per gram of tissue (%ID/g) was calculated.

Data Analysis

Data are reported as mean ± SD unless stated otherwise. *Ex vivo* biodistribution values are depicted as box-and-whisker plots (min-to-max). Statistical significance was determined by multiple *t* tests, corrected for multiple comparisons using the Holm-Sidak method, with alpha = 0.05 (GraphPad Prism).

Results

Normal Tissue Expression of hPSCA in hPSCA KI Mice

Anti-human PSCA antibodies do not cross-react with murine PSCA; therefore, a knock-in model was used to assess whether normal tissue expression would interfere with imaging contrast for anti-PSCA immuno-PET. Human PSCA expression in the hPSCA KI mouse model was confirmed by immunohistochemical staining of tissues (Fig. 1a), with the parental mouse anti-human PSCA antibody 1G8 [5]. PSCA expression is highly restricted and low levels were observed in the normal prostate, bladder, and stomach but no expression was seen in the bone, bone marrow, or lymph nodes (common sites for PCa metastasis, data not shown).

Normal Tissue Expression in hPSCA KI Mice Detected by [^{124}I]A11 Minibody Immuno-PET

Radioiodine uptake by sodium-iodide symporter (NIS) in the thyroid and the gastric mucosa was blocked prior to the imaging study. In accordance with the hPSCA expression pattern, [^{124}I]A11 Mb immuno-PET at 20 h postinjection showed higher uptake in the stomach of hPSCA KI mice compared with wild-type C57BL/6J mice (Fig. 1b). The non-residualizing tracer results in effectively no visible background. However, the catabolized [^{124}I]A11 Mb is excreted with the urine and activity can be seen in the bladder. As a result, hPSCA-specific uptake in the bladder or prostate is difficult to distinguish *in vivo*. To directly compare uptake in hPSCA-expressing organs, *ex vivo* PET

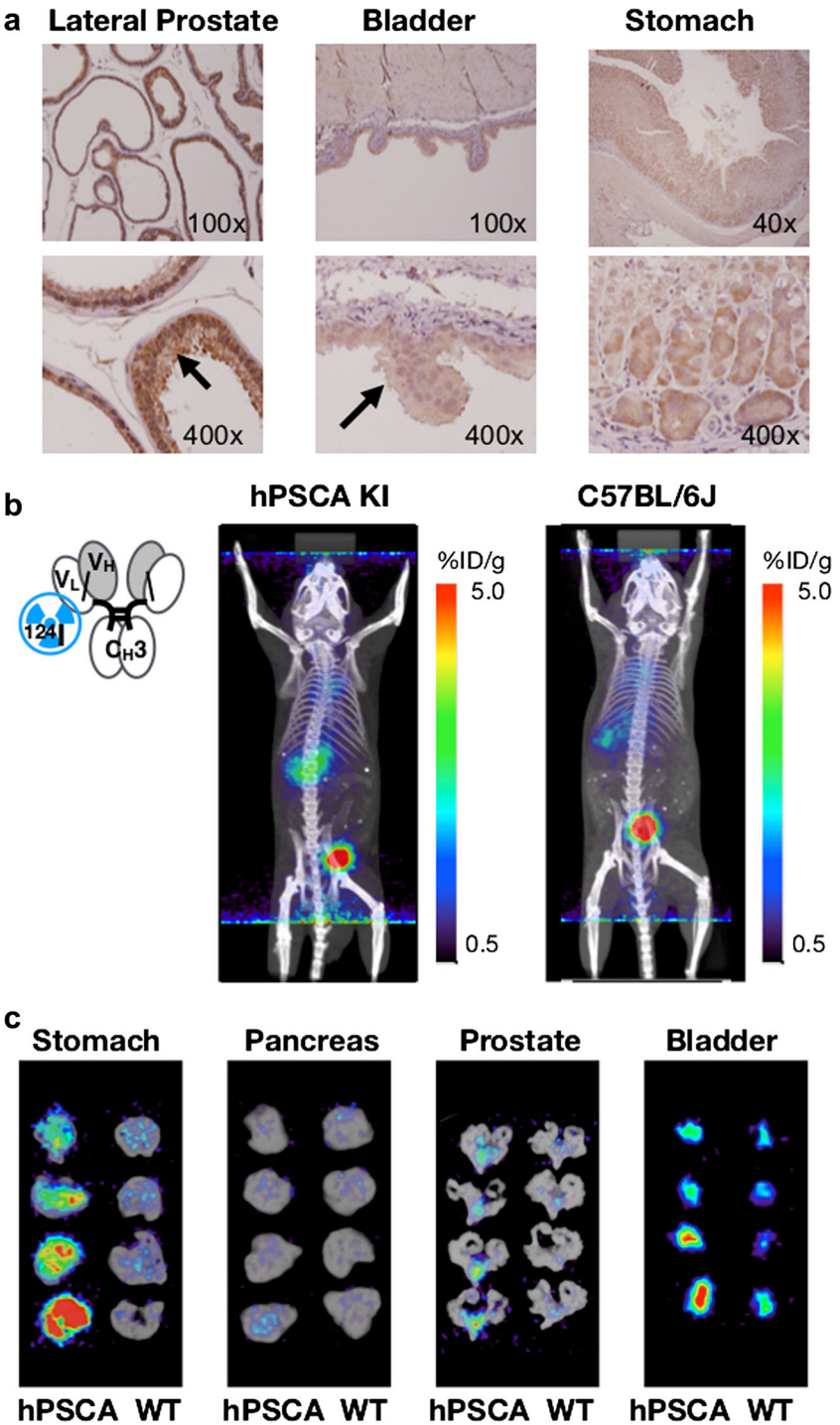

Fig. 1 hPSCA-expression in hPSCA KI mice and [^{124}I]A11 Mb immuno-PET. **a** Human PSCA knock-in mice (hPSCA KI x C57BL/6 J) show a low-level expression of PSCA in the normal prostate, bladder, and stomach similar to the expression pattern seen in humans. Immunohistochemical staining was performed with anti-hPSCA mouse mAb 1G8 (parental antibody of A11 Mb and A2cDb). **b** [^{124}I]A11 Mb (4.44 MBq/30 µg) was injected into hPSCA KI and wildtype C57BL/6J mice ($n = 4$ each) and immuno-PET scans were acquired 20 h postinjection. **c***Ex vivo* PET/CT scans of normal PSCA-expressing tissues. hPSCA KI mice (left panels) showed slightly higher tracer uptake in the stomach and the bladder compared with C57BL/6J wild-type mice (right panels).

scans were acquired of stomach, pancreas, prostate, and seminal vesicles and bladder of hPSCA KI and wild-type mice (Fig. 1c). In hPSCA KI mice, slightly higher tracer uptake was observed in the stomach, prostate, and bladder.

Uptake of [^{124}I]A11 Mb in hPSCA-Expressing Organs Is Confirmed by Ex Vivo Biodistribution

Ex vivo biodistribution of [^{124}I]A11 Mb at 44 h p.i. in hPSCA KI mice confirmed higher uptake in the stomach as seen in the *in vivo* immuno-PET scans (2.0 ± 0.2 %ID/g compared with 0.8 ± 0.1 %ID/g in wild-type C57BL/6 J) (Table 1). The differences in uptake in the other hPSCA-expressing organs (prostate and bladder), that was observed in the *ex vivo* PET scans, was also confirmed to be significantly higher in hPSCA KI mice (Table 1). I-124 radiometabolites (after catabolism of A11 Mb) are non-residualizing and hence diffuse from cells and are excreted *via* kidneys/urine, resulting in very low retention of activity in clearance organs (liver, kidney, and spleen). However, the remaining activity in the urine might obstruct the view of the prostate and together with the [^{124}I]A11 Mb circulating in the blood (5.3 ± 0.5 %ID/g) suggest that an even later time point for imaging is warranted.

Site-Specific Radiolabeling of [^{89}Zr]malDFO-A2 cDb

To investigate if a smaller antibody fragment with faster blood clearance in combination with a residualizing radiometal (retain activity in the kidneys) would enable higher prostate sensitivity at earlier imaging time points, the anti-PSCA A2 cys-diabody (A2cDb) was labeled with Zr-89. Maleimide-deferoxamine (malDFO) was conjugated to C-terminal cysteine residues of A2cDb (Fig. 2a), and site-specific conjugation was confirmed by SDS-PAGE analysis, where unconjugated A2cDb migrates at approximately 50 kDa (covalent dimer). If the C-terminal cysteine is conjugated with malDFO the formation of that disulfide bond is blocked and A2cDb-malDFO migrates at 26 kDa corresponding to the weight of the monomer (Fig. 2b). Size-exclusion analysis was performed to ensure that the conjugation did not impair the non-covalent dimeric conformation of the diabody. A2cDb-malDFO (22.1 min) eluted with a similar single-peak profile as unconjugated A2cDb (22.3 min) and at the expected elution time consistent with the 50 kDa molecular weight of the diabody (Fig. 2c).

Table 1. *Ex vivo* biodistribution 20 h post injection of [^{124}I]A11 Mb. Values are depicted as %ID/g ± SD of $n = 4$ per group

	C57BL/6J	hPSCA-KI	*p*
Prostate, Sem. Ves.	0.5 ± 0.04	0.8 ± 0.1	0.011
Bladder	1.7 ± 0.3	3.2 ± 0.4	0.009
Stomach	0.8 ± 0.1	2.0 ± 0.2	0.0004
Pancreas	0.5 ± 0.02	0.6 ± 0.1	ns
Muscle	0.4 ± 0.04	0.4 ± 0.02	ns
Liver	1.1 ± 0.03	1.2 ± 0.1	ns
Kidney	1.9 ± 0.1	2.1 ± 0.2	ns
Lung	2.8 ± 0.3	2.9 ± 0.3	ns
Spleen	1.3 ± 0.03	1.4 ± 0.2	ns
Blood	4.7 ± 0.2	5.3 ± 0.5	ns

A2cDb-DFO was subsequently radiolabeled by chelation of Zr-89, resulting in [^{89}Zr]malDFO-A2cDb ([^{89}Zr]A2cDb, $n = 3$) with a labeling efficiency of 98 ± 2 %, specific activity of 5.3 ± 0.7 μCi/μg, and radiochemical purity of 99 ± 0.8 % after size exclusion spin column. [^{89}Zr]A2cDb retained PSCA-specific binding to RM-9-hPSCA cells (immunoreactive fraction 70.9 ± 5.2 %, $n = 3$).

[^{89}Zr]A2cDb Immuno-PET Results in High-Contrast Images at Earlier Time Points

[^{89}Zr]A2cDb (55–75 μCi/12–15 μg) was injected intravenously into C57BL/6J wild-type or hPSCA KI mice and *in vivo* PET/CT images were acquired 5 and 20 h postinjection (Fig. 3a). Biodistributions were similar in both groups with renal clearance and secretion into the urine visible at 5 h and retention of activity in the kidneys due to the residualizing Zr-89. At 20 h p.i., the activity had cleared form the bladder, allowing an unobstructed view of the pelvis that would permit detection of cancer in the prostate located behind the bladder.

Ex vivo PET scans showed slightly higher activity uptake in the stomach of hPSCA KI mice while uptake in the prostate, bladder, and pancreas was indiscernible between hPSCA Ki and wild-type mice (Fig. 3b).

Specific Targeting of RM-9-hPSCA Tumors in hPSCA KI Mice Demonstrated by [^{89}Zr]A2cDb Immuno-PET

hPSCA KI mice were implanted with subcutaneous (s.c.). syngeneic grafts RM-9 (left shoulder) or RM-9-hPSCA (right shoulder). [^{89}Zr]A2cDb immuno-PET scans show rapid and specific accumulation of activity in the RM-9-hPSCA tumors at 5 h p.i. decreasing slightly until 20 h p.i. (Fig. 4). Negligible nonspecific uptake is observed in negative RM-9 tumors. These results confirm that tumor uptake is antigen specific and not significantly impaired by PSCA expression in normal tissues.

Ex Vivo Biodistribution of [^{89}Zr]A2cDb in Wild-Type, hPSCA KI and Tumor-Bearing hPSCA KI

Ex vivo biodistribution (20 h postinjection) (Fig. 5) confirmed that tumor uptake was significantly higher in RM-9-hPSCA compared with RM-9 (2.96 ± 0.7 %ID/g *vs* 1.36 ± 0.3 %ID/g, $p = 0.0049$; Table 2). The remaining activity in the blood was comparable between the four groups (0.19–0.23 %ID/g), resulting in a tumor-to-blood ratio of 12.8 (95%CI: 12.3–15.5) for the RM-9-hPSCA group. PSCA-expressing normal tissues (stomach, bladder, and prostate) showed higher uptake in hPSCA KI mice (non-tumor bearing, RM-9 and RM-9-hPSCA groups) compared with the wild-type group (C57BL/6 J); however, statistical significance was not reached. In summary, using the fast-clearing A2cDb, high-contrast immuno-PET images were achieved at earlier time

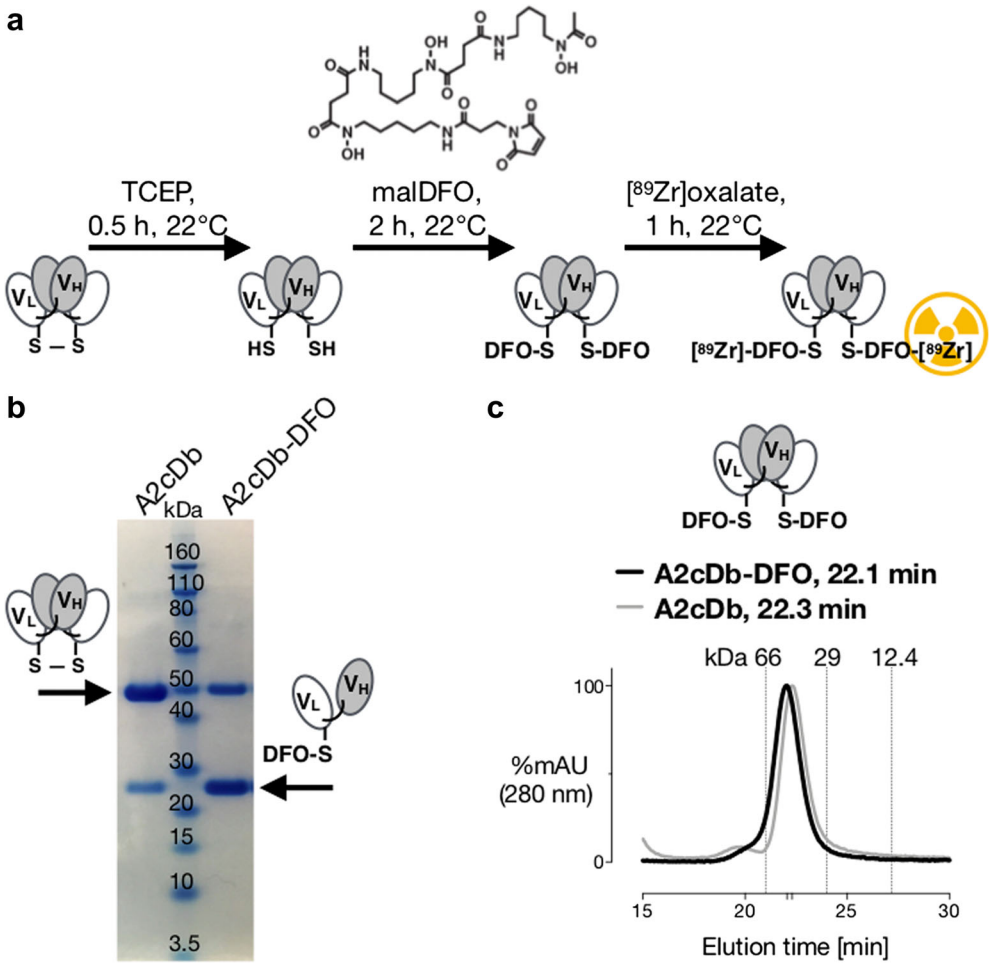

Fig. 2 Site-specific Zr-89 radiolabeling of A2 cys-diabody. **a** The A2cDb is reduced under mild conditions and conjugated site specifically with maleimide-DFO followed by chelation of Zr-89. **b** SDS-PAGE analysis shows unconjugated A2cDb (left lane) migrating at ~50 kDa. The A2cDb-malDFO migrates as monomer confirming site-specific conjugation. **c** Size-exclusion chromatography shows similar elution profiles for A2cDb and A2cDb-malDFO, confirming that malDFO conjugation does not impair the non-covalent dimeric conformation of the diabody.

points with tumor targeting and biodistribution not impacted by normal tissue expression of PSCA.

Discussion

The usefulness of targeted imaging for prostate cancer (PCa) is emphasized by the tremendous progress made in PSMA imaging [19]. However, no biomarker is 100 % sensitive and the identification of alternative targets could improve diagnosis, management, and treatment of PCa. Better understanding of tumor heterogeneity and resistance mechanisms and the ability to target more than one antigen might in the future facilitate more personalized therapies or combination therapies.

In vivo prostate cancer model systems are crucial in understanding underlying biology and in the evaluation of novel diagnostic and therapeutic strategies.

We have previously used anti-PSCA immuno-PET (A11 Mb and A2cDb) for imaging of prostate and pancreatic cancer. We showed tumor-specific tracer uptake in a variety of mouse models: subcutaneous and orthotropic xenografts, patient-derived xenografts, intratibial xenografts (mimicking bone metastases), response to androgen deprivation therapy (ADT), and in combination with fluorescence image guidance in surgical settings [10, 14, 15, 20]. However, most models require immunocompromised hosts (nude, SCID, NSG) and the immunological status (and endogenous levels of antibodies) can greatly impact antibody elimination/clearance [21, 22]. Furthermore, these mouse models do not express the target (hPSCA) in normal tissues.

In this study, anti-PSCA antibody fragments were radiolabeled (I-124 or Zr-89) and evaluated in a human PSCA knock-in mouse model (hPSCA KI) by immuno-PET and *ex vivo* biodistribution. The human PSCA knock-in model used in this study achieved biological (*i.e.*, natural) expression patterns and levels, as the expression of the mouse PSCA homolog in normal tissue is similar to that seen in humans [23]. The use of hPSCA KI mice in

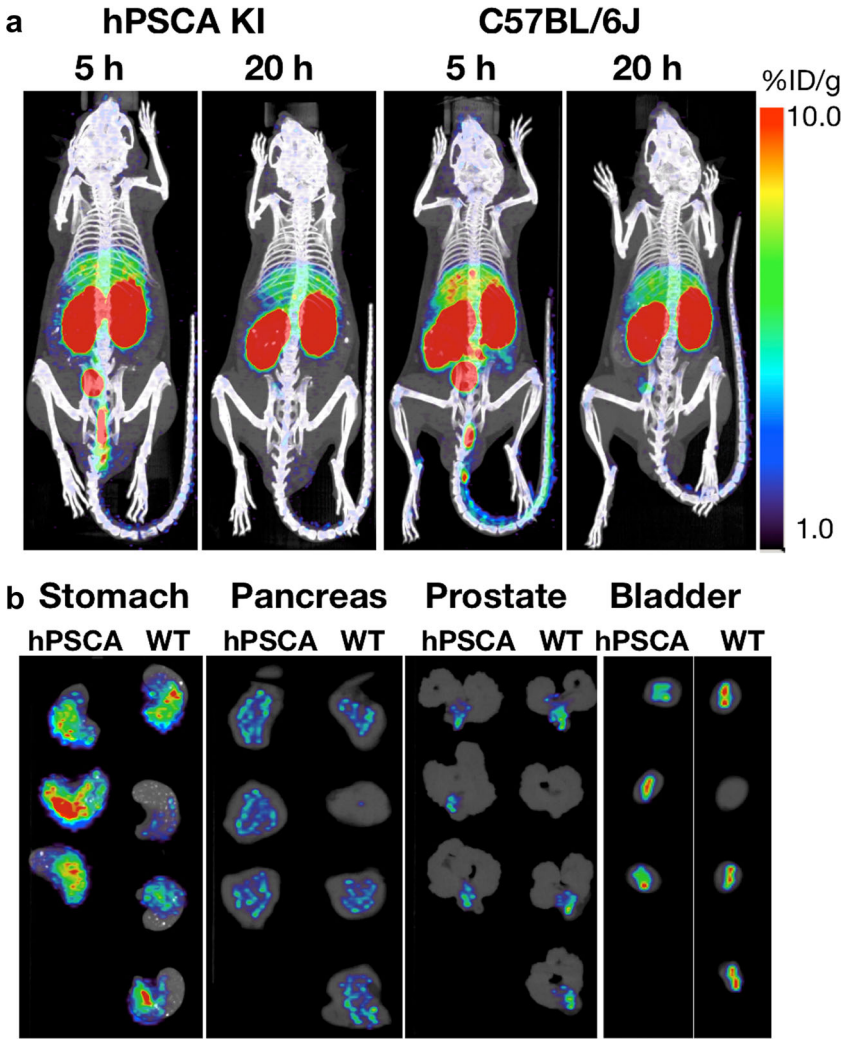

Fig. 3 [^{89}Zr]A2cDb immuno-PET of hPSCA KI mice. **a***In vivo* [^{89}Zr]A2cDb immuno-PET (2–2.8 MBq/12–15 µg, i.v. tail vein) at 5 and 20 h postinjection into hPSCA KI mice ($n = 6$) and C57BL/6J wild-type mice ($n = 4$). Scans are displayed as whole-body MIP/CT overlays. **b***Ex vivo* PET/CT scans of normal PSCA-expressing tissues. hPSCA KI mice (left panels) showed slightly higher tracer uptake in the stomach compared with C57BL/6J wild-type mice.

combination with a syngeneic mouse PCa cell line expressing hPSCA allows us to evaluate our immuno-PET tracers for cancer detection in the context of PSCA background expression and in immunocompetent mice.

In hPSCA KI mice [^{124}I]A11 Mb showed PSCA-specific uptake in normal tissues such as stomach and bladder and to a lower extent in the prostate. Despite the ability to detect small differences in PSCA expression, the longer half-life of the minibody ($t_{1/2}$ approximately 5–12 h) resulted in high remaining blood activity at 20 h p.i. and excretion of activity into the bladder (urine) proximal to the prostate that would likely complicate detection of prostate cancer [20]. The low background in the pancreas and in the liver might favor this tracer for the detection of pancreatic cancers and metastases to the liver.

[^{89}Zr]A2cDb combines a shorter half-life ($t_{1/2}$ 2–5 h) and a residualizing radiometal with the intent to achieve high-contrast images at early time points. Indeed, [^{89}Zr]A2cDb immuno-PET visualized syngeneic RM-9-hPSCA s.c. tumors as early as 5 h p.i. and retention of the radioactivity in the kidneys resulted in an unobstructed view of the pelvis within 20 h p.i., which is crucial for the detection of lesions in the prostate. Importantly, the presence of normal tissue PSCA expression did not change the biodistribution of [^{89}Zr]A2cDb significantly (at 20 h p.i.), although uptake in stomach and bladder was slightly higher in hPSCA KI mice compared with wild-type mice.

We had previously compared the two long-lived radionuclides I-124 ($t_{1/2} = 4.2$ days) an Zr-89 ($t_{1/2} = 3.3$ days) labeled to the A11 minibody (A11 Mb) for immuno-PET imaging of prostate cancer xenografts (22Rv1-PSCA and LAPC-9) in immunocompromised mice (nude and SCID) and found that the [^{124}I]A11 Mb resulted in a much higher image contrast (at 44 h p.i.) caused by the lower nonspecific

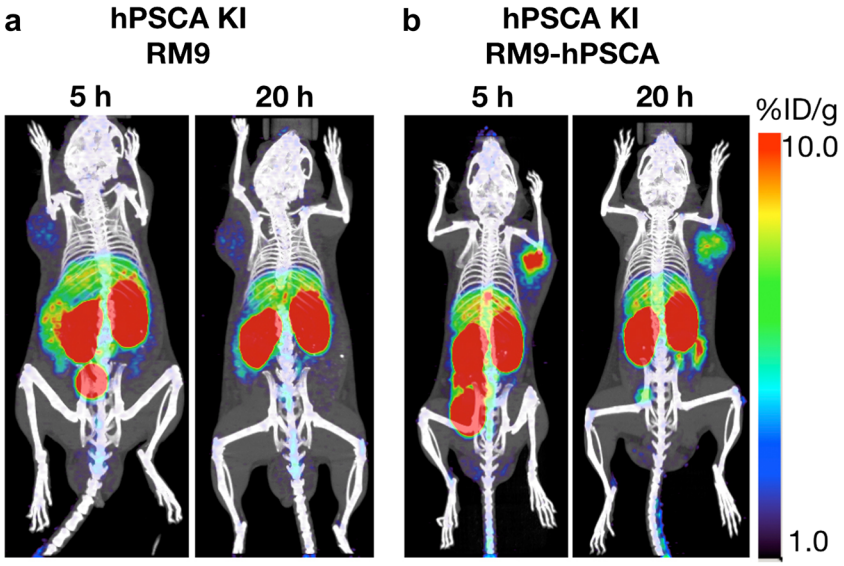

Fig. 4 [^{89}Zr]A2cDb immuno-PET of hPSCA KI mice bearing syngeneic prostate cancer tumors. [^{89}Zr]A2cDb (2–2.8 MBq/12–15 µg) was injected intravenously into hPSCA KI mice bearing **a** RM-9 (left shoulder, n = 6) or **b** RM-9-hPSCA (right shoulder, *n* = 8) subcutaneous tumors. *In vivo* PET CT images were acquired 5 and 20 h postinjection and are displayed as whole-body MIP/CT overlays. [^{89}Zr]A2cDb immuno-PET showed antigen-specific targeting of PSCA-expressing tumors (RM-9-hPSCA) and minimal nonspecific uptake in PSCA-negative RM-9 tumors. Renal clearance and excretion with urine resulted in an unobstructed view of the pelvis and lower abdomen at the 20 h time point that would allow the detection of cancer in the prostate.

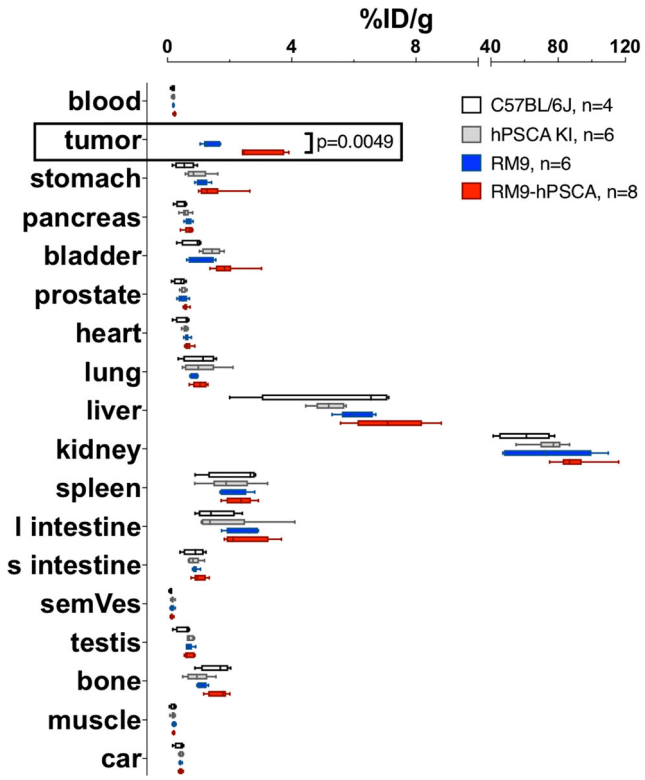

Fig. 5 *Ex vivo* biodistribution of [^{89}Zr]A2cDb, 20 h p.i. tumors and organs were harvested and gamma counted. The injected dose per gram tissue (%ID/g) was calculated based on standards containing 1 % of the ID.

tissue background of the non-residualizing radionuclide [10]. This effect is aided by the very slow internalization of PSCA in these models, while for rapidly internalizing antigens the residualizing radiometal Zr-89 might accumulate and yield higher tumor uptake.

Other advantages of using Zr-89 as a PET tracer for imaging small structures in the prostate are shorter mean positron range (1.1 mm compared with 3.0 mm for I-124) which leads to higher effective resolution and lower partial volume effect, and the fact that the emitted gamma rays (909 keV) are outside the scanners energy window (lowering background). However, for quantitation of small-animal PET images, partial-volume correction can greatly improve the correlation between PET analysis and *ex vivo* biodistribution.

While no preclinical prostate cancer model recapitulates human disease, they might each cover different aspects. Using tumor cell lines in xenograft allows for targeting of human biomarkers but bypasses tumor initiation and progression and requires immunocompromised mice as hosts. Implantation of tumor cells into immunocompromised mouse strains results in abnormal tumor microenvironment, which depends on interactions between cancer cells, the surrounding tissue and the immune system [24]. Other models, such as genetically engineered models (GEM) of prostate cancer provide tumor progression over time in the prostatic microenvironment and with a fully intact immune system. Their major disadvantages are important anatomical and biological differences in mouse *vs* human prostate, the lack of human biomarker expression and the failure of GEM

Table 2. *Ex vivo* biodistribution 20 h postinjection of [^{89}Zr]A2cDb. Values are depicted as %ID/g ± SD of $n \geq 4$ per group

	C57BL/6J $n=4$		hPSCA KI $n=6$		hPSCA KI, RM-9 $n=6$		hPSCA KI, RM-9-hPSCA $n=8$	
	Mean	SD	Mean	SD	Mean	SD	Mean	SD
Blood	0.19	0.06	0.19	0.04	0.19	0.02	0.23	0.03
Tumor	nd		nd		1.36	0.27	*2.94	0.69
Stomach	0.55	0.33	0.94	0.38	1.12	0.20	1.43	0.54
Pancreas	0.48	0.19	0.59	0.15	0.68	0.11	0.68	0.14
Bladder	0.83	0.36	1.41	0.31	1.04	0.41	1.90	0.55
Prostate	0.40	0.20	0.50	0.09	0.50	0.16	0.59	0.07
Heart	0.52	0.24	0.58	0.08	0.63	0.08	0.66	0.11
Lung	1.05	0.53	1.08	0.59	0.88	0.12	1.03	0.23
Liver	5.56	2.41	5.20	0.49	6.06	0.53	7.14	1.13
Kidney	60.4	15.6	75.0	10.7	74.3	27.9	89.6	12.3
Spleen	2.27	0.92	2.00	0.78	2.13	0.46	2.34	0.42
L. intestine	1.53	0.64	1.83	1.17	2.47	0.50	2.45	0.74
S. intestine	0.86	0.35	0.86	0.20	0.90	0.09	1.03	0.21
Sem. Ves.	0.11	0.04	0.17	0.05	0.15	0.06	0.14	0.05
Testis	0.54	0.25	0.72	0.11	0.71	0.12	0.68	0.14
Bone	1.58	0.49	0.97	0.40	1.09	0.16	1.64	0.32
Muscle	0.19	0.09	0.18	0.06	0.21	0.05	0.20	0.03
Carcass	0.39	0.16	0.43	0.06	0.42	0.03	0.43	0.06

*$p = 0.0049$

PCa models to metastasize to the bone (where 90 % of human PCa metastases occur) [25, 26]. Murine PCa syngeneic graft models in immunocompetent hosts allow to assessing the role of immune cells in the tumor microenvironment in tumor progression and resistance to therapy and are hence a mainstay for immunotherapy studies [25].

The hPSCA KI model could for example inform radioimmunotherapy studies both in terms of dosimetry (dose to PSCA expressing organs) and because radiation induces immune responses. Another important approach is orthotropic implantation of tumor cells, as the interaction between implanted cells and organ tissue of origin leads to increased metastatic potential [27]. A recent study using A11 Mb conjugated with the near-infrared dye IRDye800CW showed detection of orthotropic RM-9 hPSCA tumors and metastatic lymph nodes in hPSCA KI mice for surgical guidance [16]. While intraoperative fluorescence imaging relies on good local contrast to surrounding healthy tissues, future studies will have to show that [^{89}Zr]A2cDb immuno-PET can detect orthotropic prostate cancer and lymph node metastasis noninvasively.

Conclusions

A hPSCA knock-in mouse model in combination with syngeneic hPSCA-expressing PCa tumors enables the evaluation of targeted therapies and imaging in immunocompetent mice and in the context of normal PSCA expression. Our study revealed minimal impact of normal tissue PSCA expression on the biodistribution of two different anti-PSCA immuno-PET tracers ([^{124}I]A11 Mb and [^{89}Zr]A2cDb) and on the antigen-specific targeting of [^{89}Zr]A2cDb to hPSCA-expressing syngeneic tumors (RM-9 hPSCA). Rapid renal clearance of the 50 kDa tracer [^{89}Zr]A2cDb resulted in high-contrast PET images at early time points (4–20 h p.i.) and resulted in an unobstructed view of the lower abdomen at 20 h postinjection that would allow the detection of cancer in the prostate.

Acknowledgments. We thank Chau Tran, Jean Kimi Wang, and Johnny Guan for their technical assistance. We thank Dr. Saul Priceman for providing cell lines RM-9 and RM-9-hPSCA.

Funding Information. This work was supported by NIH grant R01 CA174294 and Department of Defense IDEA Award W81XWH-15-1-0725. Small-animal imaging and pathology core services were supported by the Jonsson Comprehensive Cancer Center (JCCC) P30 CA016042.

Compliance with Ethical Standards

Conflict of Interest

AM Wu holds ownership interest in and is a consultant/advisory board member for ImaginAb, Inc. AM Wu and RE Reiter are members of the JCCC. All other authors declare that they have no conflict of interest.

Ethical Compliance

All applicable institutional and/or national guidelines for the care and use of animals were followed. This article does not contain studies with human participants.

References

1. Sarkar S, Das S (2016) A review of imaging methods for prostate cancer detection. Biomed Eng Comput Biol 7:1–15
2. Rayn KN, Elnabawi YA, Sheth N (2018) Clinical implications of PET/CT in prostate cancer management. Transl Androl Urol 7:844–854
3. Risbridger GP, Toivanen R, Taylor RA (2018) Preclinical models of prostate cancer: patient-derived xenografts, organoids, and other explant models. Cold Spring Harb Perspect Med 8
4. Reiter RE, Gu Z, Watabe T, Thomas G, Szigeti K, Davis E, Wahl M, Nisitani S, Yamashiro J, le Beau MM, Loda M, Witte ON (1998) Prostate stem cell antigen: a cell surface marker overexpressed in prostate cancer. Proc Natl Acad Sci U S A 95:1735–1740

5. Gu Z, Thomas G, Yamashiro J, Shintaku IP, Dorey F, Raitano A, Witte ON, Said JW, Loda M, Reiter RE (2000) Prostate stem cell antigen (PSCA) expression increases with high Gleason score, advanced stage and bone metastasis in prostate cancer. Oncogene 19:1288–1296
6. Olafsen T, Gu Z, Sherman MA, Leyton JV, Witkosky ME, Shively JE, Raubitschek AA, Morrison SL, Wu AM, Reiter RE (2007) Targeting, imaging, and therapy using a humanized antiprostate stem cell antigen (PSCA) antibody. J Immunother 30:396–405
7. Wu AM, Yazaki PJ (2000) Designer genes: recombinant antibody fragments for biological imaging. Q J Nucl Med 44:268–283
8. Knowles SM, Wu AM (2012) Advances in immuno-positron emission tomography: antibodies for molecular imaging in oncology. J Clin Oncol 30:3884–3892
9. Wu AM (2014) Engineered antibodies for molecular imaging of cancer. Methods 65:139–147
10. Knowles SM, Zettlitz KA, Tavare R, Rochefort MM, Salazar FB, Stout DB, Yazaki PJ, Reiter RE, Wu AM (2014) Quantitative immunoPET of prostate cancer xenografts with ^{89}Zr- and ^{124}I-labeled anti-PSCA A11 minibody. J Nucl Med 55:452–459
11. Gu Z, Yamashiro J, Kono E, Reiter RE (2005) Anti-prostate stem cell antigen monoclonal antibody 1G8 induces cell death in vitro and inhibits tumor growth in vivo via a Fc-independent mechanism. Cancer Res 65:9495–9500
12. Leyton JV, Olafsen T, Lepin EJ, Hahm S, Bauer KB, Reiter RE, Wu AM (2008) Humanized radioiodinated minibody for imaging of prostate stem cell antigen-expressing tumors. Clin Cancer Res 14:7488–7496
13. Lepin EJ, Leyton JV, Zhou Y, Olafsen T, Salazar FB, McCabe KE, Hahm S, Marks JD, Reiter RE, Wu AM (2010) An affinity matured minibody for PET imaging of prostate stem cell antigen (PSCA)-expressing tumors. Eur J Nucl Med Mol Imaging 37:1529–1538
14. Knowles SM, Tavare R, Zettlitz KA, Rochefort MM, Salazar FB, Jiang ZK, Reiter RE, Wu AM (2014) Applications of immunoPET: using ^{124}I-anti-PSCA A11 minibody for imaging disease progression and response to therapy in mouse xenograft models of prostate cancer. Clin Cancer Res 20:6367–6378
15. Zettlitz KA, Tsai WK, Knowles SM et al (2018) Dual-modality immuno-PET and near-infrared fluorescence imaging of pancreatic cancer using an anti-prostate stem cell antigen cys-diabody. J Nucl Med 59:1398–1405
16. Zhang M, Kobayashi N, Zettlitz KA, Kono EA, Yamashiro JM, Tsai WTK, Jiang ZK, Tran CP, Wang C, Guan J, Wu AM, Reiter RE (2018) Near-infrared dye-labeled anti-prostate stem cell antigen minibody enables real-time fluorescence imaging and targeted surgery in translational mouse models. Clin Cancer Res 25:188–200. https://doi.org/10.1158/1078-0432.CCR-18-1382
17. Sonn GA, Behesnilian AS, Jiang ZK, Zettlitz KA, Lepin EJ, Bentolila LA, Knowles SM, Lawrence D, Wu AM, Reiter RE (2016) Fluorescent image-guided surgery with an anti-prostate stem cell antigen (PSCA) diabody enables targeted resection of mouse prostate cancer xenografts in real time. Clin Cancer Res 22:1403–1412
18. Loening AM, Gambhir SS (2003) AMIDE: a free software tool for multimodality medical image analysis. Mol Imaging 2:131–137
19. Donin NM, Reiter R (2017) Why targeting PSMA is a game changer in the management of prostate cancer - a urologist's point of view. J Nucl Med
20. Tsai WK, Zettlitz KA, Tavare R, Kobayashi N, Reiter RE, Wu AM (2018) Dual-modality immunoPET/fluorescence imaging of prostate cancer with an anti-PSCA cys-minibody. Theranostics 8:5903–5914
21. Vilhelmsson-Timmermand O, Santos E, Thorek DL et al (2015) Radiolabeled antibodies in prostate cancer: a case study showing the effect of host immunity on antibody bio-distribution. Nucl Med Biol 42:375–380
22. Sharma SK, Chow A, Monette S, Vivier D, Pourat J, Edwards KJ, Dilling TR, Abdel-Atti D, Zeglis BM, Poirier JT, Lewis JS (2018) Fc-mediated anomalous biodistribution of therapeutic antibodies in immunodeficient mouse models. Cancer Res 78:1820–1832
23. Raff AB, Gray A, Kast WM (2009) Prostate stem cell antigen: a prospective therapeutic and diagnostic target. Cancer Lett 277:126–132
24. Rea D, Del Vecchio V, Palma G et al (2016) Mouse models in prostate cancer translational research: from xenograft to PDX. Biomed Res Int 2016:9750795
25. Ittmann M, Huang J, Radaelli E, Martin P, Signoretti S, Sullivan R, Simons BW, Ward JM, Robinson BD, Chu GC, Loda M, Thomas G, Borowsky A, Cardiff RD (2013) Animal models of human prostate cancer: the consensus report of the New York meeting of the Mouse Models of Human Cancers Consortium Prostate Pathology Committee. Cancer Res 73:2718–2736
26. Grabowska MM, DeGraff DJ, Yu X et al (2014) Mouse models of prostate cancer: picking the best model for the question. Cancer Metastasis Rev 33:377–397
27. An Z, Wang X, Geller J, Moossa AR, Hoffman RM (1998) Surgical orthotopic implantation allows high lung and lymph node metastatic expression of human prostate carcinoma cell line PC-3 in nude mice. Prostate 34:169–174